ACS APPLIED MATERIALS & INTERFACES

Research Article

www.acsami.org

Ultrasound-Triggered Phase-Transition Cationic Nanodroplets for Enhanced Gene Delivery

Di Gao,[†,‡] Ming Xu,[§,‡] Zhong Cao,[†] Jinbiao Gao,[†] Ya Chen,[†] Yingqin Li,[†] Zhe Yang,[†] Xiaoyan Xie,[§] Qing Jiang,[†] Wei Wang,*[,§] and Jie Liu*[,†]

[†]Department of Biomedical Engineering, School of Engineering, Sun Yat-sen University, Guangzhou, Guangdong 510006, China

[§]Department of Medical Ultrasonics, Institute of Diagnostic and Interventional Ultrasound, The First Affiliated Hospital of Sun Yat-sen University, Guangzhou, Guangdong 510080, China

Supporting Information

ABSTRACT: Ultrasound as an external stimulus for enhanced gene transfection represents a safe, noninvasive, cost-effective delivery strategy for gene therapy. Herein, we have developed an ultrasound-triggered phase-transition cationic nanodroplet based on a novel perfluorinated amphiphilic poly(amino acid), which could simultaneously load perfluoropentane (PFP) and nucleic acids. The heptadecafluoroundecylamine ($C_{11}F_{17}$-NH_2) was chosen to initiate β-benzyl-L-aspartate *N*-carboxyanhydride (BLA-NCA) ring-opening polymerization to prepare $C_{11}F_{17}$-poly(β-benzyl-L-aspartate) ($C_{11}F_{17}$-PBLA). Subsequently, $C_{11}F_{17}$-poly{*N*-[*N*′-(2-aminoethyl)]aspartamide} [$C_{11}F_{17}$-PAsp(DET)] was synthesized by aminolysis reaction of $C_{11}F_{17}$-PBLA with diethylenetriamine (DET). PFP/pDNA-loaded nanodroplets PFP-TNDs [PFP/$C_{11}F_{17}$-PAsp(DET)/LucDNA/γ-PGA or poly(glutamic acid)-*g*-MeO-poly(ethylene glycol) (PGA-*g*-mPEG) ternary nanodroplets] were primarily formulated by an oil/water emulsification method, followed by surface modification with PGA-*g*-mPEG. The average diameter of PFP-TNDs ranged from 300 to 400 nm, and transmission electron microscopy images showed that the nanodroplets were nearly spherical in shape. The ζ potential of the nanodroplets dramatically decreased from +54.3 to +15.3 mV after modification with PGA-*g*-mPEG, resulting in a significant increase of the stability of the nanodroplets in the serum-containing condition. With ultrasound irradiation, the gene transfection efficiency was enhanced 14-fold on HepG2 cells, and ultrasound-triggered phase-transition cationic nanodroplets also displayed a good ultrasound contrast effect. These results suggest that the PFP/DNA-loaded phase-transition cationic nanodroplets can be utilized as efficient theranostic agents for targeting gene delivery.

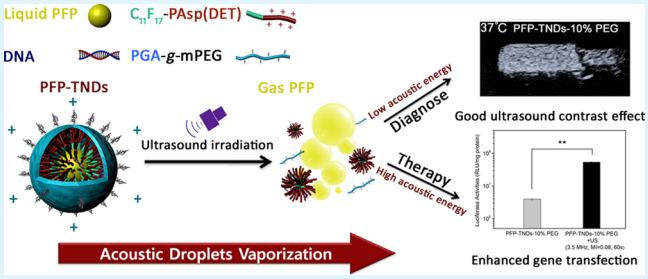

KEYWORDS: *nanodroplets, gene transfection, perfluoropentane, ultrasound, acoustic droplet vaporization, cavitation*

1. INTRODUCTION

Gene therapy, as one of the powerful strategies for cancer treatments, has attracted wide attention with the development of molecular biology in the past decade. In order to protect and control the release of the gene to the target location in time, secure and effective gene-delivery systems are urgently needed. Although viral gene-delivery vectors have been recognized as exquisite gene carriers to realize efficient gene transfection,[1,2] they are possibly unsafe, leading to severe immunological inflammation or even carcinomatosis in patients.[3−5] Cationic polymers such as poly(ethylenimine) (PEI),[6] poly(amino esters),[7] poly(amino acid),[8] polyamide,[9−11] and chitosan[12] occupy important positions in the process of gene-delivery system development. However, insufficient suppression of cancer cell growth and migration remains a major challenge because of the low gene transfection efficiency and the complexity of cancers.[13,14] Therefore, preferable gene-delivery strategies should be investigated and implemented to improve the effectiveness of gene therapy.

In recent years, applications of ultrasound (US) as an external stimulus to enhance the gene transfection efficiency have been demonstrated because of its safe, noninvasive, and cost-effective features for site-specific targeting, overmatching the other physical methods.[15,16] Therein, microbubbles in association with US are capable of delivering DNA systemically along with the controlled release of DNA at special target locations after sonication.[17] Because of cavitation and microjets/jetstreams caused by microbubble oscillation and more violent microbubble collapse under US irradiation, the permeability of cell membranes increases, accompanied by facilitated cellular uptake, resulting in enhanced gene transfection efficiency.

To increase the colocalization of DNA and microbubbles after intravenous injection at the target site and reduce

Received: April 1, 2015
Accepted: May 28, 2015
Published: May 28, 2015

© 2015 American Chemical Society

DOI: 10.1021/acsami.5b02832
ACS Appl. Mater. Interfaces 2015, 7, 13524−13537

Scheme 1. Illustrative Preparation of US-Triggered Phase-Transition Cationic Nanodroplets PFP-TNDs and the Process of US-Assisted Gene Transfection

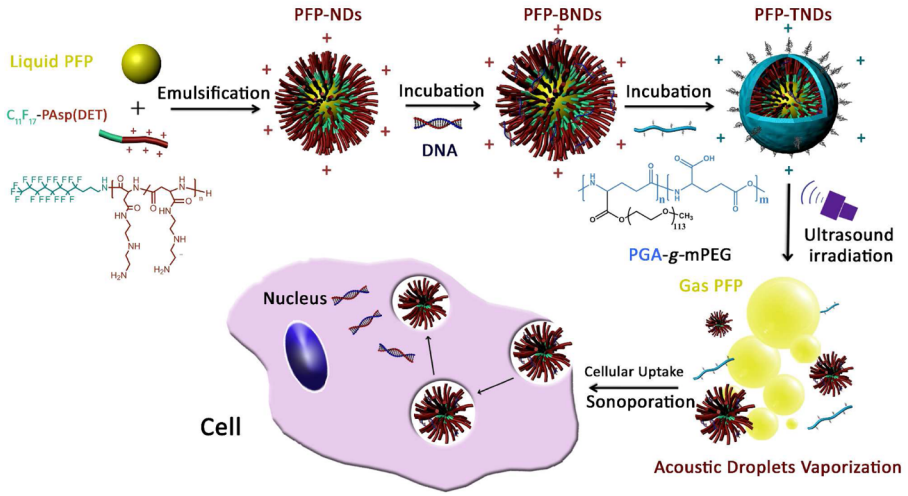

extracellular nucleases of released DNA, a variety of gene-delivery strategies have been designed.[18−21] Endo-Takahashi and co-workers successfully developed cationic poly(ethylene glycol) (PEG)-modified bubble liposomes (BLs) to achieve the codelivery of DNA and perfluoropropane gas. The results indicated that BLs in cooperation with US irradiation can be used as an efficient tool to realize gene delivery in vitro and in vivo.[19] Additionally, Shuai and co-workers reported a different method for realizing not only high small interfering RNA (siRNA) transfection efficiency under US-targeted microbubble destruction but also an effective siRNA protection that is a nanoparticulate heteroassembly of the siRNA-loaded positive polymeric micelles and negative liposomes.[20]

However, previous studies revealed that the large size of the microbubbles (>1 μm) prevented them from passing through the endothelial gaps of tumor blood vessels via the enhanced permeability and retention (EPR) effect.[15] Furthermore, microbubbles carrying gas-phase perfluorocarbon (PFC) showed poor resistance to physics distortion and sonication, leading to a short circulation time in vivo.[22] Hence, liquid-phase PFC nanoemulsions have been sought as replacements.[23,24] Nanodroplets, utilizing liposomes[25,26] and polymers[24] to load a low-boiling-point liquid PFC, could remain in their liquid state at body temperature until irradiated by US with fully high acoustic pressure to induce acoustic droplet vaporization (ADV) into microbubbles. This special character of alternative acoustic activation enables the droplets to perform the both diagnostic imaging and therapy. For diagnostic purposes, liquid PFC nanodroplets can be vaporized to generate gas bubbles to markedly enhance acoustic impedance for ultrasonography.[27,28] Therapeutically, nanodroplets have been investigated as efficient tools for potentiating aberration correction,[29] high-intensity focused US sensitization,[30,31] and drug delivery.[32] However, combining liquid PFC encapsulation and DNA condensation in a single nanocarrier for gene delivery has not been reported yet.

In this study, we report an efficient theranostic nanovehicle for targeting gene delivery developed on the basis of US-triggered phase-transition cationic nanodroplets. As for the structure of this cationic nanodroplets, first, a new kind of cationic polymer, $C_{11}F_{17}$-poly{*N*-[*N*′-(2-aminoethyl)]aspartamide} [$C_{11}F_{17}$-PAsp(DET)], was synthesized not only to efficiently load the perfluoropentane (PFP) resulting from the high compatibility of PFP and the hydrophobic perfluorinated segment in the polymer but also to provide a hydrophilic cationic segment for DNA binding. Then, the anionic polymer poly(glutamic acid)-*g*-MeO-poly(ethylene glycol) (PGA-*g*-mPEG) was selected to modify the surface of the DNA-loaded cationic nanodroplets to enhance the biocompatibility and serum stability (Scheme 1). The nanodroplet structure was determined by dynamic light scattering (DLS) and transmission electron microscopy (TEM). In vitro studies were conducted to evaluate the US sensitivity, DNA delivery ability, cellular uptake, and gene transfection against HepG2 cells with or without US irradiation.

2. MATERIALS AND METHODS

2.1. Materials. 1*H*,1*H*,2*H*,2*H*,3*H*,3*H*-Perfluoroundecylamine ($C_{11}F_{17}$-NH_2), triphosgene, chloroform-*d* ($CDCl_3$), dimethyl sulfoxide-d_6 (DMSO-d_6), deuterium oxide (D_2O), Hoechst 33342, and 3-(4,5-dimethyl-2-thiazolyl)-2,5-diphenyl-2*H*-tetrazolium bromide (MTT) were purchased from Sigma Co. β-Benzyl-L-aspartate acid (BLA) was purchased from GL Biochem (Shanghai) Ltd. and used as received. Diethylenetriamine (DET) and *N*-methyl-2-pyrrolidone (NMP) were obtained from Aladdin Industrial Co. (China) and used after conventional distillation. Micro-BCA protein assay was purchased from Thermo Fisher Scientific Inc. Poly(γ-glutamic acid) (γ-PGA; 5000 Da) was obtained from Nanjing Sai Taisi Biotechnology Co. Ltd. (China). Perfluoro-*n*-pentane (PFP) was obtained from Strem Chemicals, Inc. MeO-poly(ethylene glycol)-NH_2 (mPEG-NH_2; 3000 Da) was bought from Jenkem Technology Co. Ltd. A Label IT Tracker Intracellular Nucleic Acid Kit was obtained from Mirus Co. Gel red was obtained from Biotium Inc. pLucDNA (pGL4.13 encoding the firefly luciferase), luciferase assay buffer, and reporter lysis buffer were purchased from Promega Co. Branched poly(ethylenimine) (PEI; 25 kDa) was purchased from Sigma-Aldrich Trading Co., Ltd. HepG2 cells and LLC cells were purchased from Shanghai Cell Bank of the Chinese Academy of Sciences and cultured in Dulbecco's modified Eagle's medium (Hyclone), supplemented with 10% (v/v) fetal bovine serum (FBS) and 1% (w/v) penicillin−streptomycin (PS) in a 5% CO_2-humidified atmosphere at 37 °C.

2.2. Synthesis of β-Benzyl-L-aspartate *N*-Carboxyanhydride (BLA-NCA). BLA-NCA was synthesized by phosgenation of BLA using triphosgene through the Fuchs-Farthing method.[33,34] Briefly, BLA (5 g) was reacted with triphosgene (3.1 g, about 1.4 equiv) in 60 mL of anhydrous tetrahydrofuran under a nitrogen atmosphere at 50 °C for 15 min until the solution became clear. The reaction was

DOI: 10.1021/acsami.5b02832
ACS Appl. Mater. Interfaces 2015, 7, 13524−13537

continue for another 20 min under a nitrogen atmosphere to remove the generated chlorine hydride and excess triphosgene. Then anhydrous *n*-hexane was slowly added to the solution until the appearance of BLA-NCA crystals. The solution was placed at −20 °C overnight to fully crystallize. To purify BLA-NCA, the primary products were dissolved in anhydrous acetic ether and precipitated by *n*-hexane at least three times. Finally, the white needlelike BLA-NCA crystals were dried in vacuo in the presence of phosphorus pentoxide (P_2O_5) and NaOH powder for the polymerization.

2.3. Synthesis of $C_{11}F_{17}$-poly(β-benzyl-L-aspartate) ($C_{11}F_{17}$-PBLA). $C_{11}F_{17}$-PBLA was prepared through the BLA-NCA ring-opening polymerization (ROP) method with the initiator $C_{11}F_{17}$-NH_2. Briefly, BLA-NCA (1.2 g) was first dissolved in 6 mL of an anhydrous 1/5 (v/v) dimethylformamide (DMF)/dichloromethane (DCM) mixture. $C_{11}F_{17}$-NH_2 (0.046 mL) diluted with DCM (2 mL) was slowly dropped into BLA-NCA. The chemical reaction was kept at 25 °C for at least 3 days under a dry nitrogen atmosphere. Then, the solution was dialyzed against DMF for 1 day and against deionized water for another 2 days before lyophilization to obtain the white powder $C_{11}F_{17}$-PBLA. The synthesized $C_{11}F_{17}$-PBLA was stored at −20 °C.

2.4. Synthesis of $C_{11}F_{17}$-poly{*N*-[*N*′-(2-aminoethyl)]-aspartamide} [$C_{11}F_{17}$-PAsp(DET)]. To synthesize $C_{11}F_{17}$-PAsp(DET) via aminolysis reaction, $C_{11}F_{17}$-PBLA (300 mg) and DET (2 mL) were first dissolved in 5 and 2 mL of NMP, respectively. Then DET was slowly dropped into $C_{11}F_{17}$-PBLA to react for 6 h at 25 °C, followed by injection of a 1 M HCl aqueous solution (20.2 mL) in an ice−water cooling bath. The mixture solution was dialyzed against a 0.01 M HCl aqueous solution for 1 day and then against deionized water for another 2 days. The final solution was freeze-dried to get $C_{11}F_{17}$-PAsp(DET), which was stored at −20 °C.

2.5. Polymer Characterization. The chemical structures of the products of each step were determined by proton nuclear magnetic resonance (^{1}H NMR) spectroscopy recorded with a 400 MHz Bruker AvanceIII spectrometer. For the solvent choice, BLA-NCA was dissolved in $CDCl_3$ and $C_{11}F_{17}$-PBLA was dissolved in DMSO-d_6, whereas $C_{11}F_{17}$-PAsp(DET) was detected by dissolving the polymers in D_2O. Additionally, the molecular weight of each polymer was calculated by integrating the area of the characteristic peak on the spectra.

2.6. Preparation of PFP-NDs. The PFP-NDs [PFP/$C_{11}F_{17}$-PAsp(DET) nanodroplets] were formulated by an ordinary oil/water (o/w) emulsification method. Specifically, cationic polymer $C_{11}F_{17}$-PAsp(DET) was first dissolved in 2 mL of deionized water with a polymer concentration of 5 mg/mL, and the mixture was kept at 4 °C for 10 min. Then, 60 μL of PFP (3%, v/v) was slowly added to the bottom of a $C_{11}F_{17}$-PAsp(DET) aqueous solution. The precooling solution was subsequently transferred into an ice bath equipped with a probe-type sonicator (Misonix Sonicator S-4000) while undergoing a probe sonication process (30% amplitude, 1 s power on, 1 s power off, 90 s). The acquired PFP-NDs were stored at 4 °C for less than 4 h prior to use.

2.7. Preparation of Multiple Component Nanodroplets PFP-BNDs and PFP-TNDs. The PFP-BNDs [PFP/$C_{11}F_{17}$-PAsp(DET)/LucDNA binary nanodroplets] and subsequent surface-modified ternary nanodroplets PFP-TNDs [PFP/$C_{11}F_{17}$-PAsp(DET)/LucDNA/γ-PGA or PGA-*g*-mPEG ternary nanodroplets] were prepared by the following steps. It is worth noting that the N/P/C ratio signals the molar ratio of the primary amine groups in the N-substituted polyaspartamides to the phosphate groups in plasmid to the dissociative carboxyl in γ-PGA or PGA-*g*-mPEG. Typically, the binary nanodroplets PFP-BNDs was primarily formulated by gentle mixing of the plasmid DNA and PFP-NDs at a N/P ratio of 20 in deionized water, followed by 30 min of incubation at 4 °C. Then, to prepare the PFP-TNDs at different C/N ratios, a certain amount of PGA-*g*-mPEG or γ-PGA dissolved in a 10% glucose solution was added to an equal volume of a PFP-BNDs aqueous solution to adjust the glucose concentration to 5% (isosmotic solution). Subsequently, the resultant solution was completely mixed by vortex and further incubated for 30 min at 4 °C to generate PFP-TNDs. The acquired echogenic PFP-BNDs and PFP-TNDs were reserved at 4 °C for less than 4 h before use.

2.8. Characterization of PFP-BNDs and PFP-TNDs. Through DLS measurement using a Malvern Zetasizer Nano ZS90, the particle size and ζ potential of PFP-NDs, PFP-BNDs, and PFP-TNDs were analyzed. Each sample was determined at 25 °C after being diluted in deionized water. The morphology of the nanodroplets, negatively stained by an aqueous solution of uranyl acetate, was directly determined by a transmission electron microscope (JEM 1400).

The temperature-related particle size of PFP-TNDs was scaled by increasing the temperature from 25 to 75 °C with a heating rate of 5 °C/min. Also, to directly observe the particle size, an optical microscope (DM2500p, Leica) equipped with 40× focal lens and temperature-controlled stages (THMS600, Linkam) was used.

2.9. Dye Exclusion Assay. Gel red exclusion assay was chosen to evaluate the DNA condensation ability of PFP-BNDs and PFP-TNDs as previously report.[35] Specifically, the nanodroplet solution was first mixed with an aliquot of the gel red solution (100×), followed by incubation at 25 °C for 10 min in the dark. As a control, a naked DNA solution containing an equal amount of DNA was selected to experience the same experimental steps. Then, a microplate reader (BioTek Synergy 4) was used to measure the fluorescence intensity of the samples with an excitation wavelength of 510 nm and an emission wavelength of 590 nm. Next, the following equation was used to calculate the relative fluorescence intensity of the nanodroplets:

$$\text{relative fluorescence (\%)} = \frac{F_{\text{sample}} - F_{\text{gel red}}}{F_{\text{DNA}} - F_{\text{gel red}}} \times 100\%$$

where F_{sample}, $F_{\text{gel red}}$, and F_{DNA} stand for the fluorescence intensities of the nanodroplets, gel red, and naked DNA, respectively.

2.10. Nanodroplet Stability Studies. Through observation of the size variation of PFP-BNDs and PFP-TNDs in a mimic physiological condition in vitro, the stability of the nanodroplets was evaluated. Typically, the nanodroplets were first diluted by a PBS/FBS solution [0.01 M, pH = 7.4, 10% (v/v) FBS] before gentle rotation (37 °C). Then, 100 μL of the nanodroplets was removed from the solution to analyze the size distribution by DLS at different time points. All measurements were conducted in triplicate.

2.11. In Vitro US Imaging. US imaging in vitro was conducted in Plastic Pasteur pipettes (with an inner diameter of 10 mm) filled with a PFP-TNDs solution (with degassed water used as the dilution medium) before being immersed into a degassed water tank. Focused US was generated by a diagnostic Aplio500 (Toshiba Medical Systems, Tokyo, Japan) equipped with a 3 cm × 1 cm transducer head (375BT). Besides, pulsed US (pulse length 250 ms and mean frequency 4 kHz) was used to perform contrast-enhanced ultrasonography (CEUS) imaging at different frequencies and mechanical index (MI) values. For subsequent analysis and processing by *ImageJ* software, all images and videos were kept digitally. As for the groups measured at 37 °C, the images were recorded after 20 s of heating of the PFP-TNDs−10% PEG solution.

2.12. Acoustic Stability of Incorporated DNA. To assess the DNA binding ability of PFP-BNDs and PFP-TNDs after US irradiation, the nanodroplets (3 μg of DNA per sample) were prepared and exposed to US at various MI values. After sonication, the nanodroplets were resuspended in 2 μL of the DNA loading buffer and added into the wells of a 1% (w/v) agarose gel containing 0.1 μL/mL gel red. Then, electrophoresis was performed in a triacetate−ethylenediaminetetraacetic acid buffer (pH = 7.4) for 45 min with a voltage of 100 V, followed by fluorescence-related visualization under UV irradiation.

To investigate the integrality of DNA after sonication, DNA was eluted from the nanodroplets by adding 10 μL of heparin (30 IU/μg of DNA). After incubation for 4 h, the integrity of the plasmid in each formulation was analyzed by agarose gel electrophoresis as described above. Naked DNA and untreated PFP-BNDs and PFP-TNDs were presented as controls.

2.13. In Vitro Gene Transfection Studies. *Optimization of PFP-BNDs and PFP-TNDs.* To screen out the optimal N/P ratios for

DOI: 10.1021/acsami.5b02832
ACS Appl. Mater. Interfaces 2015, 7, 13524−13537

PFP-BNDs, the nanodroplets were studied at different N/P ratios ranging from 5 to 35 against HepG2 cells. Briefly, 5×10^4 HepG2 cells were seeded in each well of a 48-well plate and cultured in a complete medium (37 °C, 5% CO_2) to allow the cells to adhere. Then, the nanodroplets (0.5 μg of LucDNA per sample) were added to each well. As a positive control, a PEI/LucDNA polyplex was selected at the same time. After 6 h of incubation, the medium was changed to a fresh one for another 42 h of incubation. For luciferase assay, the HepG2 cells were first washed twice by PBS, followed by lysis in 100 μL of a 1× reporter lysis buffer. The cell lysate was centrifuged in an eppendorf tube (12000 rpm, 10 min), and 20 μL of supernatant was blended with 100 μL of a luciferase assay buffer. Meanwhile, the fluorescence intensity (by relative light units or RLU) was detected by a luminometer. Furthermore, the BCA protein assay kit was used to measure the protein level and the gene transfection efficiency was shown as RLU/mg of protein.

For the PFP-TNDs, the influence of the γ-PGA and PGA-*g*-mPEG coating on the gene transfection efficiency was investigated at various C/N molar ratios between 2/5 and 10/5. The luciferase gene transfection efficiency of the nanodroplet samples was detected in accordance with the procedures described above, and all of the transfection experiments were conducted in triplicate.

Transfection of PFP-TNDs−10% PEG with US Irradiation. In order for the cells to be immediately exposed to US through placement of a ultrasonic probe (375BT, 3.0 cm in length and 1.0 cm in width) in the well, a density of 2×10^5 cells/well of HepG2 cells was seeded in a 6-well plate and cultured overnight in 2 mL of the complete growth medium. The nanodroplets containing 2 μg of LucDNA were added to each well before US irradiation. During the period of US exposure, the US parameters including frequency and MI values as well as the exposure time were adjusted. At 6 h after US irradiation, the medium was changed back to 2 mL of the complete medium, and the cells were incubated for a total of 48 h. Untreated PFP-TNDs−10% PEG was used as the control. The luciferase gene transfection efficiency of the nanodroplets was detected in accordance with the procedures described previously.

2.14. Cellular Uptake. First, for cellular uptake studied by a flow cytometer, plasmid DNA with fluorescence labeling was first prepared according to the manufacturer's protocol of a Label IT Tracker Intracellular Nucleic Acid Localization Kit (Mirus, Madison, WI), for which fluorescein was conjugated to the plasmid. Second, a density of 2×10^5 cells/well of HepG2 cells was seeded in a 6-well plate and incubated overnight in 2 mL of the complete growth medium. Subsequently, PFP-BNDs and PFP-TNDs containing 2 μg of fluorescein-labeled DNA were added to each well. After US exposure (the same method described in the section of gene transfection), the cells were incubated at 37 °C for another 4 h. As for the postprocessing steps, the medium was removed, primarily followed by rinsing of the cells with a PBS solution (0.01 M, pH = 7.4) three times. Then, trypsin was used to digest the cells, which were further harvested through centrifugation at 1500 rpm for 5 min. After the cells were resuspended in 0.5 mL of precooling PBS, the fluorescein contents of the cells in each well were analyzed by FACS Callibur (Becton Dickinson) and the excitation wavelength was set to 488 nm (10000 counts for each measurement).

Confocal laser scanning microscopy (CLSM) was selected to further observe the cellular uptake of nanodroplets containing fluorescence-labeled DNA by HepG2 cells. Cells were seeded in a 6-well plate (2×10^5 cells/well density) and incubated overnight in 2 mL of the complete growth medium. Different nanodroplets containing 2 μg of plasmid were incubated with the cells before US irradiation, and the cells were incubated for another 4 h. Then the medium was removed, followed by rinsing of the cells with a PBS solution (0.01 M, pH = 7.4) three times. The cell nuclei were stained by Hoechst 33342 (10 μg/mL), and fluorescein-labeled DNA was observed using a spectral confocal microscope (Leica TCS SP5). The excitation wavelengths for measuring Hoechst 33342 and fluorescein were 405 and 492 nm, respectively.

2.15. In Vitro Cytotoxicity of PFP-Loaded Nanodroplets. To determine the cytotoxicity of PFP-loaded nanodroplets carrying LucDNA formulations, HepG2 cells were used to determine the cytotoxicity of PFP-BNDs and PFP-TNDs by MTT assay. Cells were seeded in a 96-well plate at a density of 7×10^3 cells/well and incubated overnight in 200 μL of the complete growth medium. Thereafter, the nanodroplets were added to the cells at different concentrations and further incubated for a total of 48 h. Subsequently, the medium was removed, followed by rinsing of the cells with a PBS solution (0.01 M, pH = 7.4) three times. Then, the medium was changed to 100 μL of fresh medium containing 20 μL of a MTT solution (5 mg/mL in PBS) and further incubated at 37 °C for another 4 h. The supernatant in each well was removed, and 150 μL of DMSO was added to dissolve the formazan salt crystals. After gentle agitation for 5 min, the absorbance at 570 nm in each well was measured using a microplate reader (BioTek Synergy 4).

Considering the effects of US irradiation on the cell viability, HepG2 cells at a density of 2×10^5 cells/well were seeded in a 6-well plate. After incubation overnight in the complete growth medium, the samples (PFP-TNDs−10% PEG, 2 μg of DNA/sample) were added, followed by US exposure under different US parameters and exposure times. Thereafter, the cells were incubated for another 48 h, and the cell viability was quantified by the MTT assay described above.

2.16. Erythrocyte Agglutination and Hemolysis Assay. To prepare the erythrocytes, healthy human blood was centrifuged at 2500 rpm for 5 min and then the isolated erythrocytes were washed with a PBS solution three times at 4 °C. For the erythrocyte agglutination study, erythrocytes were gently resuspended with PBS at a density of 2×10^6 cells/mL and the different concentrations of the nanodroplets were mixed with the erythrocyte suspension with a polymer concentration of 20 μg/mL, followed by incubation for 1 h at 37 °C. After incubation, 10 μL of the solution was dripped onto a glass slide to determine erythrocyte agglutination via a microscope.

For the hemolysis study, nanodroplets of different concentrations were added to the erythrocyte (1×10^8 cells/mL), followed by incubation at 37 °C for 1 h. The release of hemoglobin was measured after centrifugation (1500 rpm for 5 min) by photometric analysis of the supernatant at 410 nm using a microplate reader. Triton X-100 (0.1%, w/v) and isosmotic PBS were chosen as the positive and negative controls, respectively.

2.17. Statistical Analysis. Comparisons between two groups were statistically analyzed using a two-sided Student's *t* test and statistical studies between multiple groups using multiway analysis of variance (ANOVA). All data are expressed as the mean ± standard error of the mean of more than three repeated experiments. When the *P* value was <0.05, the difference was considered statistically significant.

3. RESULTS AND DISCUSSION

3.1. Synthesis and Characterization of Cationic Polymer $C_{11}F_{17}$-PAsp(DET). The fluorinated polymers with high liquid PFC compatibility were developed in a previous work.[36,37] With this inspiration, $C_{11}F_{17}$-NH_2 was first chosen as the initiator for the ROP of BLA-NCA to introduce the fluorinated groups to polymer $C_{11}F_{17}$-PBLA. Then, cationic $C_{11}F_{17}$-PAsp(DET) was synthesized through the aminolysis reaction using DET. The chemical reaction of $C_{11}F_{17}$-PAsp(DET) is shown in Scheme 2. The structures of $C_{11}F_{17}$-PBLA and $C_{11}F_{17}$-PAsp(DET) were analyzed by ^{1}H NMR spectroscopy. In Figure 1A, the resonance at δ 6.16 attributed to −N*H*− in the five-membered ring of BLA-NCA disappeared, which indicated the successful ROP of BLA-NCA. Meanwhile, the appearance of a resonance at δ 1.63 for $-CH_2CH_2CH_2-$ absorptions in terminal $C_{11}F_{17}$-NH− confirmed the function of the initiator during the ROP. Additionally, the degree of polymerization was calculated from the following proton resonance absorptions: absorptions in $-CH_2CH_2CH_2-$ at δ 1.63 mentioned above and $C_6H_5CH_2-$ at δ 7.25. After integration, the number of repeated unites was 28.2 and the corresponding molecular weight equaled 6500 D, as basically

DOI: 10.1021/acsami.5b02832
ACS Appl. Mater. Interfaces 2015, 7, 13524−13537

Scheme 2. Synthetic Scheme of $C_{11}F_{17}$-PAsp(DET)

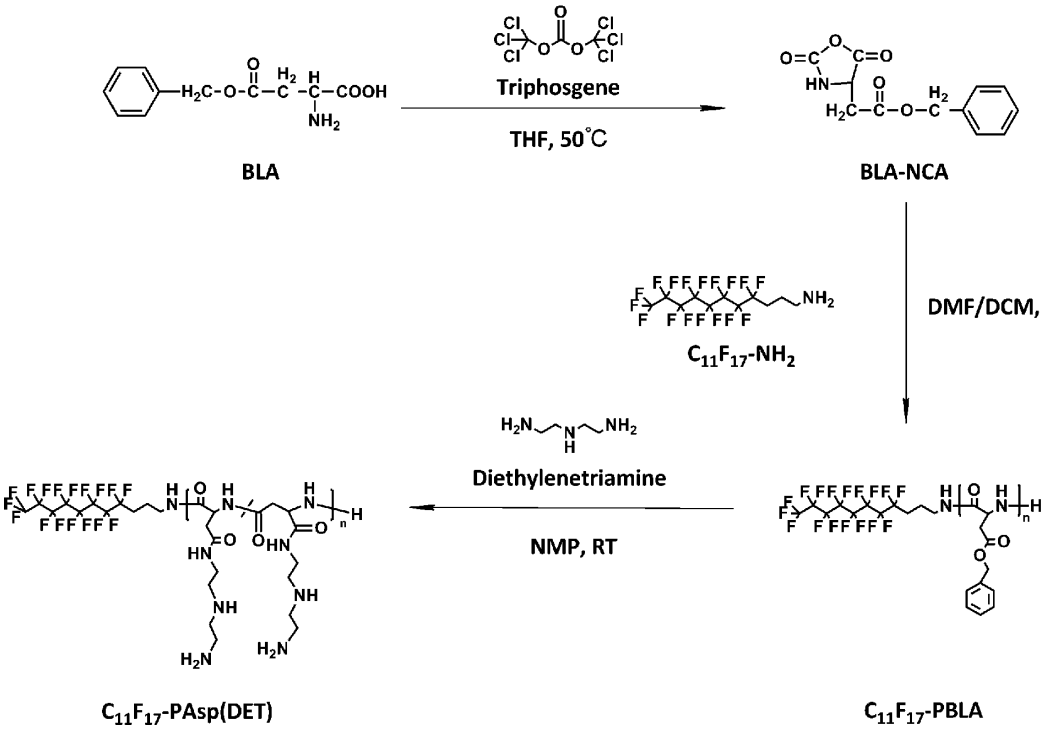

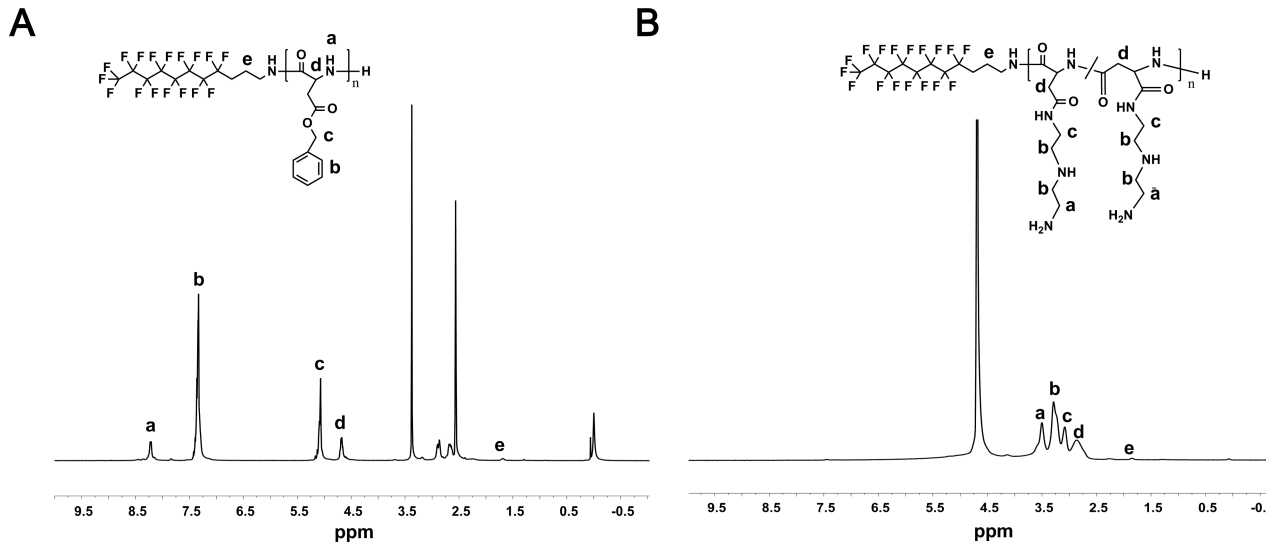

Figure 1. ^{1}H NMR spectra of (A) $C_{11}F_{17}$-PBLA in DMSO-d_6 and (B) $C_{11}F_{17}$-PAsp(DET) in D_2O (temperature, 25 °C; polymer concentration, 5 mg/mL).

designed. Figure 1B confirmed the successful aminolysis of $C_{11}F_{17}$-PBLA based on the appearance of resonance absorptions for $-CO(NHCH_2CH_2)_2$-NH_2 at δ 2.86−3.50 and the disappearance of proton resonance absorptions of the benzyl ester at δ 4.67−7.33. Besides, considering the possible breaking of main-chain amido bonds during the aminolysis reaction, the degree of polymerization and molecular weight of the obtained $C_{11}F_{17}$-PAsp(DET) had also been calculated from ^{1}H NMR spectroscopy through absorptions for $-CH_2CH_2CH_2-$ in the initiator at δ 1.63 and $-CO(NHCH_2CH_2)_2$-NH_2 in the side chains at δ 2.86−3.50. The results indicated that there was no obvious bond breaking during the aminolysis reaction.

3.2. Preparation and Optimization of PFP-Loaded Nanodroplets. The PFP-loaded $C_{11}F_{17}$-PAsp(DET) nanodroplets (PFP-NDs) were prepared by an o/w emulsification method. As shown in Figure 2A, $C_{11}F_{17}$-PAsp(DET) could be dissolved in deionized water to obtain a transparent liquid in the first place. After the addition of PFP into the solution and the subsequent probe sonication process, the solution transferred to opalescent and maintained this state over 24 h. Comparably, without the addition of the synthesized polymer $C_{11}F_{17}$-PAsp(DET) in deionized water, the same sonication process could only generate faintish opalescence and the resultant dispersion of naked PFP droplets would congregate at the bottom of the glass bottles within a short time. Additionally,

DOI: 10.1021/acsami.5b02832
ACS Appl. Mater. Interfaces 2015, 7, 13524−13537

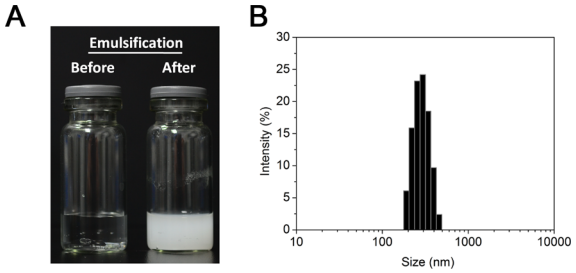

Figure 2. (A) Photograph of a PFP-NDs solution before and after emulsification through a probe sonication method. (B) Size distribution of PFP-NDs measured by DLS.

we measured the size distribution and surface charges of the prepared PFP-NDs through DLS. As illustrated in Figure 2B, there was a single peak size distribution of fabricated PFP-NDs with average diameter and zeta potential of 315 ± 22 nm and 68.5 ± 1.84 mV, respectively (Table 2). Therefore, it was confirmed that amphiphilic $C_{11}F_{17}$-PAsp(DET) definitely played a vital role in loading PFP, while the prepared positive PFP-NDs were ideal candidates to electrostatically condense negative DNA.

Following the preparation of positive nanodroplets, LucDNA and PFP-NDs were mixed to form a series of PFP/$C_{11}F_{17}$-PAsp(DET)/LucDNA binary nanodroplets (PFP-BNDs) at various N/P ratios, an influential factor for DNA binding and gene transfection.[35,38] First the incorporation of LucDNA into PFP-NDs was confirmed by gel retardation assay. The results revealed that complete DNA retardation was achieved at a N/P ratio above 1.25. To further screen the optimal N/P ratio for PFP-BNDs transfection, a luciferase report gene transfection experiment of PFP-BNDs at different N/P ratios against HepG2 cells was conducted. Figure 3A showed that the luciferase expression levels of PFP-BNDs increased with increasing N/P ratios from 5 to 20 but began to decline and continued on this downward track at N/P ratios from 25 to 35. According to the results described above, the optimal N/P ratio of 20 was selected for all subsequent experiments.

Nanoparticles carrying strong positive charge are generally not stable in physiological fluids, leading to a short in vivo circulation time. Therefore, it is essential to lower the positive charges of the particles to increase the in vivo stability of the prepared cationic nanodroplets PFP-BNDs (+54.3 mV for N/P = 20). In this study, γ-PGA, a natural poly(amino acid) with negative charges, was first employed to surface-modify the positive PFP-BNDs. The amount of γ-PGA was varied at different C/N ratios. As shown in Table 1, raising the amount of γ-PGA decreased the surface charge of the PFP/$C_{11}F_{17}$-PAsp(DET)/LucDNA/γ-PGA ternary nanodroplets (PFP-TNDs−0% PEG) from +54.3 to −28.9 mV. These results indicated that γ-PGA was successfully covered on the surface of PFP-BNDs. Besides, the mean sizes of the PFP-TNDs decreased from 414 to 318−344 nm upon modification with γ-PGA.

To realize the efficient passive targeted delivery of nanodroplets into solid tumors through the EPR effect, it is necessary to decrease the particle size to less than 400 nm in

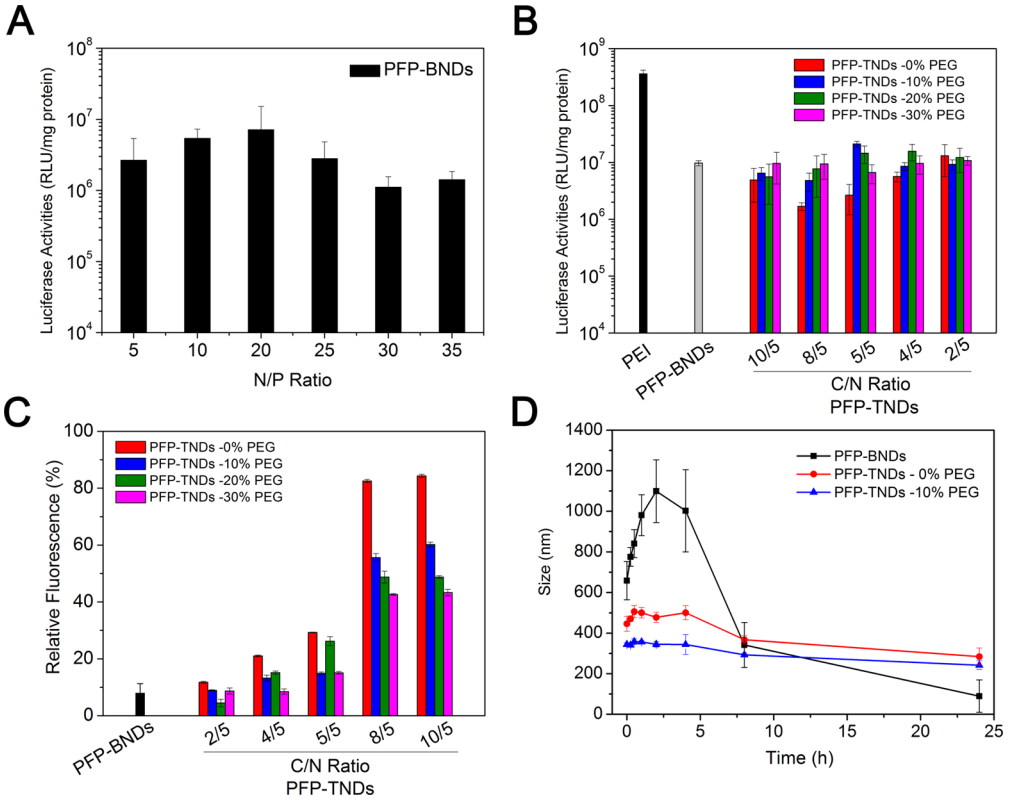

Figure 3. Gene transfection efficiency and stability of the PFP-BNDs and PFP-TNDs: (A) transfection efficiency of the PFP-BNDs with different N/P ratios on HepG2 cells; (B) transfection efficiency of the PFP-TNDs with 0−30% PEG grafting at various C/N ratios on HepG2 cells and with the PEI/DNA complex included for comparison; (C) DNA binding ability of PFP-BNDs and PFP-TNDs (with different PEG contents and C/N ratios) measured by gel red exclusion assay; (D) serum stability for the PFP-loaded nanodroplets with a N/P ratio of 20 and a C/N ratio of 5/5 incubated in a PBS/FBS solution. Data are shown as the mean ± standard deviation (n = 3).

DOI: 10.1021/acsami.5b02832
ACS Appl. Mater. Interfaces 2015, 7, 13524−13537

Table 1. Characterization of PFP-TNDs−0% PEG at Various C/N Ratios[a]

C/N ratio[b]	size (nm)	PDI	ζ potential (mV)
10/5	344 ± 36	0.187	−28.9 ± 5.8
8/5	342 ± 30	0.118	−6.4 ± 3.7
5/5	335 ± 22	0.159	13.4 ± 4.7
4/5	342 ± 39	0.243	21.7 ± 6.1
2/5	318 ± 26	0.228	28.6 ± 8.2
0[c]	414 ± 29	0.187	54.3 ± 3.6

[a]Data are shown as mean ± standard deviation (n = 3). [b]Molar ratio of carboxyl in γ-PGA to primary amine groups in the N-substituted polyaspartamides. [c]PFP/$C_{11}F_{17}$-PAsp(DET)/LucDNA binary nanodroplets (PFP-BNDs) at a N/P ratio of 20.

diameter.[39,40] On the basis of the previous researches, one of the most efficient ways to extend the blood circulation time is to introduce PEG onto the surface of the nanoparticles. However, excessive PEGylation also confines particles to interaction with cells and decreases the cellular uptake.[35,41] In this study, PGA-*g*-mPEG by grafting 10−30% PEG to γ-PGA (see our previous work for the synthetic method[41]) was utilized to surface-modify the PFP-BNDs to formulate PFP/$C_{11}F_{17}$-PAsp(DET)/LucDNA/PGA-*g*-mPEG ternary nanodroplets (e.g., PFP-TNDs−10% PEG). Figure 3B displays the gene transfection efficiency of PFP-TNDs with different PEGylation at several C/N ratios on HepG2 cells. For the ternary nanodroplets PFP-TNDs with PGA-*g*-mPEG modification, most of the samples presented similar or even higher luciferase gene transfection efficiency compared to PFP-BNDs. At a C/N ratio of 5/5, PFP-TNDs−10% PEG is nearly 2.2-fold higher than that of PFP-BNDs, and this increase could be explained by the fact that the cellular uptake of PFP-TNDs experienced a γ-PGA-specific, receptor-mediated endocytosis process relevant to the GGT receptors on the membrane of HepG2 (GGT positive cell line).[42,43] For comparison, LLC cells with much lower GGT expression were chosen as a negative cell line to test the targeting efficacy of γ-PGA- and PGA-*g*-mPEG-modified PFP-TNDs (Figure S3 in the Supporting Information, SI). It was found that the PFP-TNDs with the highest gene transfection efficiency (1.18×10^7 RLU/mg of protein for PFP-TNDs−10% PEG at C/N = 2/5) presented even lower luciferase gene transfection efficiency when compared to binary nanodroplets PFP-BNDs (1.71×10^7 RLU/mg protein), which confirmed that the PGA or PGA-*g*-mPEG modification played an important role in promoting gene transfection against the GGT positive cell line. Moreover, with further increasing PEG grafting percentage, there was a slight decrease of the gene transfection efficiency presumably attributed to lower cellular uptake rates of nanodroplets caused by excessive PEGylation. Note that the PFP-TNDs−0% PEG showed significantly lower luciferase protein expressions at most of the C/N ratios selected in the experiment in comparison with the PGA-*g*-mPEG-modified PFP-TNDs possibly because of the instability of the nanodroplets without PEGylation.[41] On the basis of these results, the PFP-TNDs with a 10% PEG graft and the C/N ratio of 5/5 were selected for subsequent studies.

The ability of cationic polymers of strong DNA binding is important for preparing nanodroplets with efficient gene transfection. To determine whether modification with γ-PGA and PGA-*g*-mPEG affects the DNA binding ability of the PFP-TNDs, a dye exclusion assay was performed. In this experiment, gel red was added to the free DNA or DNA-loaded nanodroplets and the fluorescence of dye molecules could be remarkably enhanced after being intercalated to the DNA bases. Therefore, the high fluorescence reflects the production of free plasmid DNA, while the weak fluorescence signal is detected when DNA is condensed to cationic polymer chains because of the prevented effective dye−DNA interactions.[41,44] As shown in Figure 3C, the PFP-TNDs exhibited significantly higher fluorescence intensity than the PFP-BNDs at a high C/N ratio (e.g., C/N = 8/5), which could be due to the destruction of electrostatic interactions between cationic PFP-NDs and DNA by adding excessive anionic γ-PGA. Additionally, as for the PFP-TNDs at lower C/N ratios (<5/5), the relatively low fluorescence intensity revealed that moderate surface modification did not affect the DNA condensation, which coincided with the results of the luciferase gene transfection studies. Furthermore, we have also analyzed the DNA binding ability of nanodroplets by agarose gel electrophoresis. In Figure S4 in the SI, the PFP-TNDs−10% PEG (N/P = 20) did not present the evident naked DNA band at all of the C/N ratios after modification of PGA-*g*-mPEG, which confirmed that surface modification of PGA-*g*-mPEG did not affect the DNA condensation for PFP-TNDs.

Figure 3D shows the serum stability of PFP-BNDs, PFP-TNDs−0% PEG, and PFP-TNDs−10% PEG under mimic physiological conditions in vitro. Upon incubation in a PBS/FBS solution at 37 °C for 24 h, the average size of the ternary nanodroplets PFP-TNDs modified with γ-PGA or PGA-*g*-mPEG remained nearly steady throughout the incubation period. However, the particle size of the binary nanodroplets PFP-BNDs increased rapidly from 658 to 1099 nm in the first 2 h and then experienced a sharp decrease to less than 100 nm after 24 h. Meanwhile, for the PFP-BNDs, the mean count rate value relevant to the nanodroplet concentration decreased from the primary 177 to 47 kcps finally. These results were consistent with our previous study of the cationic-polymer-based PPMS/DNA gene-delivery system, which presented that particles with excessive positive surface charges are usually unstable in physiological fluids, and the introduction of the PEG layer to nanoparticles improves this unstable situation dramatically.[35] Note that although the boiling point of PFP is 29 °C, remaining liquid at room temperature but gasifying at body temperature, when the amphiphilic polymer $C_{11}F_{17}$-PAsp(DET) is used to formulate the nanodroplets, PFP does not vaporize at body temperature, attributed to the Laplace pressure applied at the boundary of the nanodroplets. This allowed the nanodroplets to remain nanodroplets for more than 24 h at 37 °C rather than microbubbles.[24,45]

Eventually, the morphology and physicochemical characteristics of the optimal nanodroplets with different formulations are shown in Table 2 and Figure 4, respectively. The mean size

Table 2. Characterization of PFP-NDs and the optimal PFP-BNDs and PFP-TNDs−10% PEG

sample[a]	size (nm)	PDI	ζ potential (mV)
PFP-NDs	315 ± 22	0.051	68.5 ± 1.8
PFP-BNDs	414 ± 29	0.247	54.3 ± 3.6
PFP-TNDs−10% PEG	359 ± 18	0.112	15.3 ± 2.4

[a]PFP-NDs, PFP-BNDs, and PFP-TNDs−10% PEG represent PFP/$C_{11}F_{17}$-PAsp(DET) nanodroplets, PFP/$C_{11}F_{17}$-PAsp(DET)/LucDNA binary nanodroplets, and PFP/$C_{11}F_{17}$-PAsp(DET)/LucDNA/PGA-*g*-mPEG (10% PEG grafting) ternary nanodroplets, respectively.

DOI: 10.1021/acsami.5b02832
ACS Appl. Mater. Interfaces 2015, 7, 13524−13537

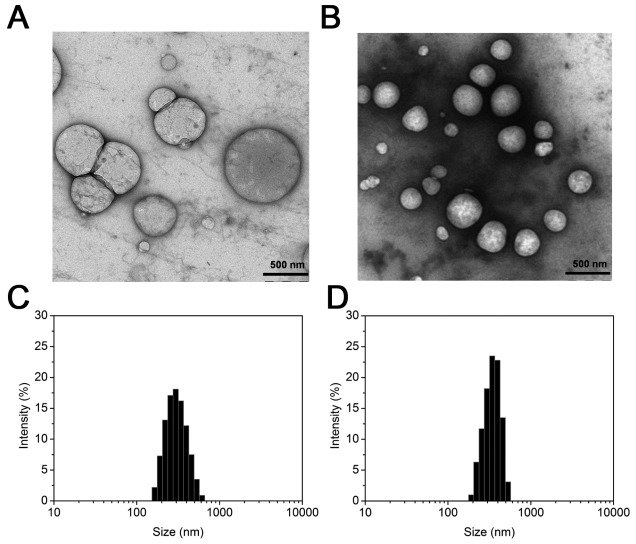

Figure 4. TEM pictures and particle size distributions of PFP-BNDs (A and C) and PFP-TNDs−10% PEG (B and D).

of PFP-TNDs−10% PEG is desirably 359 ± 18 nm, which dramatically decreased the size of the binary nanodroplets PFP-BNDs of 414 ± 29 nm because PGA-*g*-mPEG was capable of compressing the shell materials of the nanodroplets through electrostatic interaction. Moreover, for changes of the ζ potential, after incubation for a period of 20 min, the surface positive charges of PFP-NDs were neutralized by LucDNA when prepared by the PFP-BNDs, resulting in a great decrease of the ζ potential from +68.5 to about +54.3 mV. Then, there was a further decline of the surface positive charges of the obtained PFP-TNDs (+15.3 mV) attributed to modification of the anionic PGA-*g*-mPEG (Table 2). TEM images showed that the PFP-BNDs and PFP-TNDs−10% PEG were almost spherical in shape and the PFP-TNDs−10% PEG possessed a narrower particle size distribution than the PFP-BNDs (Figure 4A,B), which was consistent with the results of the sizes of both nanodroplet samples confirmed by DLS analysis (Figure 4C,D). On the basis of the results discussed above, there is an indication that the nanodroplets modified with the PGA-*g*-mPEG show the advantages of decreasing the diameter of PFP-BNDs, reducing the positive surface charges, and increasing the serum stability; therefore, the optimal ternary nanodroplets PFP-TNDs−10% PEG were selected for subsequent experiments.

3.3. Temperature-Dependent Behaviors of PFP-TNDs. In order to evaluate the PFP vaporization retardation effect of a sturdy PFP-TNDs−10% PEG shell, the changes of the size of the nanodroplets at various temperatures were visualized by optical microscopy equipped with a temperature-controlled stage. As shown in Figure S1 in the SI, although the PFP-TNDs−10% PEG underwent a gradual expansion process with increasing temperature, their structural robustness had obviously been presented. At lower temperatures (25 and 37 °C), the amount of heat was insufficient to vaporize nanodroplets, resulting in no detectable microbubbles in the images. When the temperature was continuously increased to 44 °C, microbubbles were generated with a size distribution about 10 μm. Then, the increase of the diameters of microbubbles was directly proportional to the rise of the temperature, demonstrating that the external temperature significantly affected the phase transition of PFP. It was interesting that, during the generation and expansion of microbubbles, the bubbles inclined to adhere with each other and the smaller ones could be rapidly "swallowed" by the larger ones, similar to the results of previous research.[46] This phenomenon can be presumably explained by the fact that the strong hydrophobic interaction of PFP gas in the core of generated microbubbles improves the fusion between them. Besides, the result also indicated that the polymer shell composed of $C_{11}F_{17}$-PAsp-(DET), LucDNA, and PGA-*g*-mPEG possessed well flexibility because of no immediate explosion of these microbubbles.

Temperature-dependent behaviors of PFP-TNDs−10% PEG highlighted two advantages of these phase-transition nanodroplets. First, the relative stability of the nanodroplets at the body temperature allowed prolonged systemic circulation of the PFP-TNDs because of the nanosized property. Second, the structural robustness of the polymer shell of the nanodroplets resulted in retardation of gas release, which is crucial for echo-contrast enhanced imaging after US irradiation.

3.4. In Vitro US imaging. In vitro US imaging of PFP-TNDs−10% PEG was investigated in plastic pasteur pipettes (with an inner diameter of 10 mm) by the Aplio500 system (Toshiba, Japan), which was equipped with CEUS imaging modes. Besides, different US parameters, including the temperature, frequency, and MI, were taken into consideration. Specifically, the prepared PFP-TNDs−10% PEG was diluted in degassed water to a concentration of 500 μg/mL, matching the concentration used in vivo. According to the previous researches of Rapoport and co-workers,[47] only stable bubbles may create sufficient US contrast in tumor tissues, and the US-induced phase transition (ADV) is highly desirable for both drug delivery and ultrasonography attributed to significant differences among the acoustic impedance for water (1.4 MRayl), PFP droplets (∼0.3 MRayl), and bubbles (≪0.3 MRayl). Actually, there are two factors regarded to influence the droplet-to-bubble transition including thermal (heating) and acoustic (thermal and/or mechanical). Therefore, it is necessary to investigate these factors comprehensively.

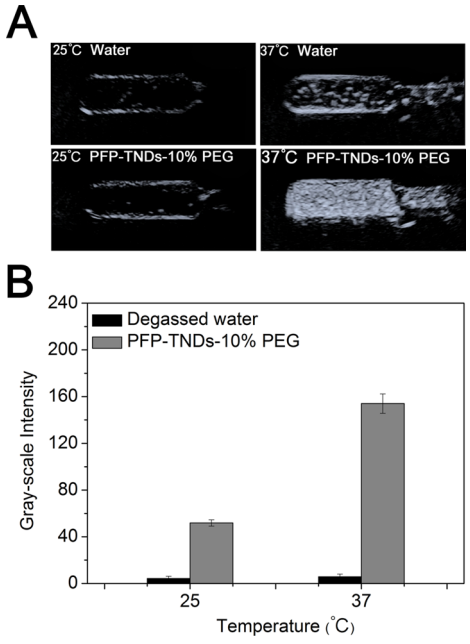

Figure 5. In vitro US images (A) and gray-scale intensities (B) of degassed water (control group) and PFP-TNDs−10% PEG diluted in degassed water (500 μg/mL) at different temperatures (frequency of 3.5 MHz and MI of 0.08).

DOI: 10.1021/acsami.5b02832
ACS Appl. Mater. Interfaces 2015, 7, 13524−13537

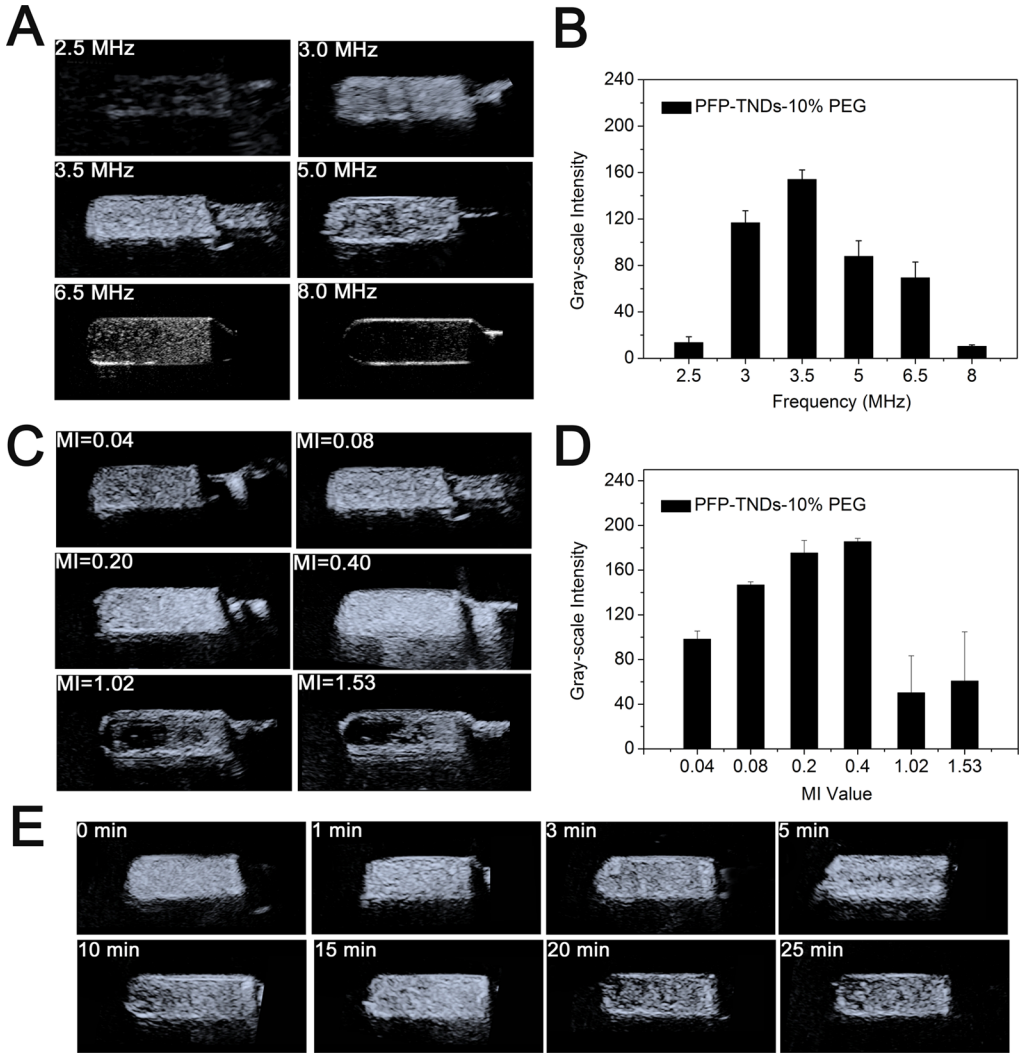

Figure 6. In vitro US images and gray-scale intensities of PFP-TNDs−10% PEG in degassed water with a concentration of 500 μg/mL at various frequencies (A and B; MI = 0.08) and MI values (C and D; frequency of 3.5 MHz) under CEUS imaging. (E) In vitro US images of PFP-TNDs−10% PEG (500 μg/mL) in degassed water detected at different imaging time points (frequency of 3.5 MHz and MI of 0.08).

First, we detected possible influences of the temperature (thermal) during US irradiation. From Figure 5A, a remarkably brighter US imaging can be obtained for PFP-TNDs−10% PEG after the temperature was enhanced from 25 to 37 °C, while there was only slight enhancement of the brightness for degassed water at the same experimental conditions. The gray-scale intensities on the images for degassed water and PFP-TNDs−10% PEG before and after the temperature was increased are presented in Figure 5B, analyzed by *ImageJ* software. The results confirmed that US-triggered phase-transition cationic nanodroplets have a good US contrast effect at 37 °C (body temperature), while the temperature played an important role in decreasing the ADV threshold for improvement of the phase transition.

Second, the influence of the US frequency on the ultrasonography was detected to select the more suitable frequency for PFP-TNDs. On the basis of preceding researches,[48,49] the resonant frequency of a microbubble is directly related to its size. The microbubbles of different diameters possess their own optimal frequency to achieve resonance for enhancing the backscattering signal and prolongating the ultrasonic imaging. As shown in Figure 6A, US imaging obtained at a frequency of 3.5 MHz was relatively brighter compared with the images measured at other frequencies under CEUS mode. After analysis of the gray-scale intensity of the obtained images by *ImageJ* software, the intensity first increased and then decreased with increasing frequency, peaking at a frequency of 3.5 MHz (Figure 6B). These results demonstrated that the frequency of 3.5 MHz is more suitable for the ultrasonography of PFP-TNDs−10% PEG under CEUS mode, so this frequency was selected to conduct the following experiments.

As an efficient theranostic agent for targeting gene delivery, the PFP-TNDs−10% PEG should experience an effective phase transition to generate enough stable microbubbles for ultrasonic diagnosis at a relatively lower MI value.[50] Meanwhile, the higher MI, utilized to enhance inertial cavitation, considered to induce the collapse of microbubbles to generate the stronger microjet proved to be the crucial factor for sonoporation. Therefore, the MI of US irradiation has been investigated for the US-triggered phase transition. The CEUS images were recorded at different MI values from 0.04 to 1.53. Figure 6C demonstrated that clear images could be obtained at MI values from 0.04 to 0.4, brightening gradually, as confirmed by the gray-scale intensity analysis in Figure 6D. However, when the

DOI: 10.1021/acsami.5b02832
ACS Appl. Mater. Interfaces 2015, 7, 13524−13537

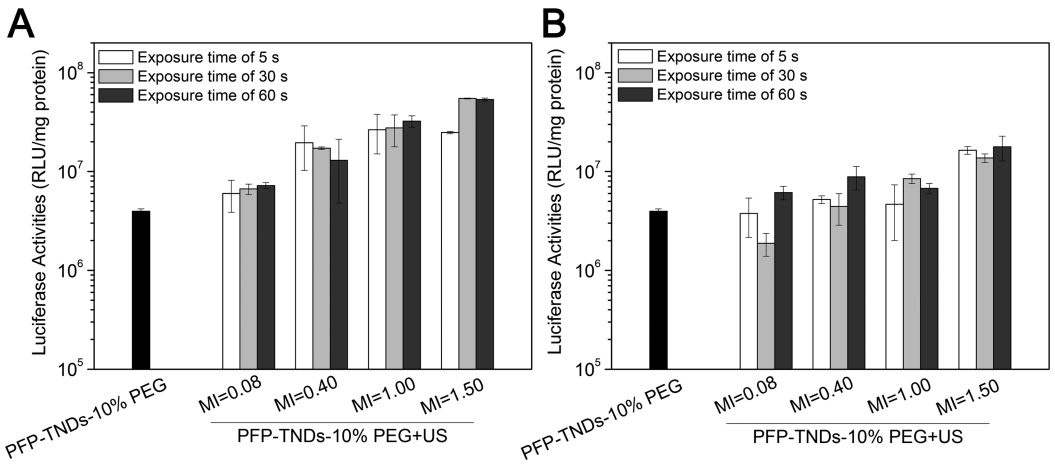

Figure 7. Luciferase expression by HepG2 cells transfected with LucDNA using PFP-TNDs−10% PEG and US at ultrasonic frequencies of 3.5 MHz (A) and 2.5 MHz (B) (n = 3).

MI value was continuously raised, the images darkened and the gray-scale intensity decreased significantly, possibly indicating that the generated microbubbles were destroyed at these MI values, leading to a decrease in the number of microbubbles. Moreover, the PFP-TNDs−10% PEG was very stable with sonication and could be continuously imaged for more than 25 min in vitro (Figure 6E). Thereby, these results demonstrated that PFP-TNDs showed great potential to act as an effective ultrasound contrast agent (UCA) for ultrasonic diagnosis.

3.5. Acoustic Stability of Incorporated DNA. On the basis of analysis of the US images above, at higher MI values (1.02 and 1.53), the generated microbubbles possibly experienced collapse and the integrality of PGA-*g*-mPEG-modified microbubbles was compromised, so it is important to detect whether the DNA could still be bound by carriers to make sure there is normal cellular uptake through the interaction between the negative cell membrane and positive gene carriers. The ability for cationic nanodroplets PFP-TNDs−10% PEG and PFP-BNDs to incorporate DNA after US irradiation was assessed by agarose gel electrophoresis, and the results are shown in Figure S2A in the SI; the absence of naked DNA bands shows that no DNA was released from both nanodroplets at different MI values. The presence of bright bands around the negative electrode shows that DNA could still be adhered by the cationic polymer $C_{11}F_{17}$-PAsp(DET) through electrostatic interaction despite the explosion of generated microbubbles.

Additionally, because US could damage DNA at extreme conditions,[51,52] we evaluate the stability of DNA after sonication. To make sure that the DNA within the nanodroplets still remained intact, the DNA molecules were displaced by heparin after sonication.[53] Subsequently, the released DNA was analyzed by agarose gel electrophoresis, which showed that the DNA helical structure was protected over the range of conditions used in this study (Figure S2B in the SI).

3.6. Gene Transfection of PFP-TNDs−10% PEG with the Aid of US Exposure. To evaluate the cavitation ability of PFP-TNDs−10% PEG, which has been proposed as a driving force for enhancing gene transfection, we transfected LucDNA using HepG2 cells under different US parameters including the MI, ultrasonic exposure time, and ultrasonic frequency.

First, to determine whether the ultrasonic frequency significantly influences the gene transfection efficiency, two frequencies of 2.5 and 3.5 MHz were investigated. In vitro US imaging showed that a visible difference of the US contrast effect could be observed for these two frequencies (Figure 6A,B), which means that it is more conducive to generate microbubbles for cavitation at 3.5 MHz. As our hypothesis, the gene transfection efficiency enhanced dramatically for most of the PFP-TNDs−10% PEG at 3.5 MHz (Figure 7A), while there was only a slight increase at 2.5 MHz (Figure 7B).

Then, our studies assessed the effect of the MI on gene transfection by changing the US's MI value between 0.08 (widely used in clinical diagnosis) and 1.50 (which was the maximum pressure of the transducer used). At a frequency of 3.5 MHz, the gene transfection efficiency enhanced significantly with an increase of the MI value and obtained a 14-fold increase over the PFP-TNDs−10% PEG without US irradiation at a MI value of 1.50. Although there was a lower transfection efficiency for a frequency of 2.5 MHz compared with that of 3.5 MHz, the same tendency could still be observed by the fact that the transfection efficiency reached a peak with a 4.5-fold increase over the PFP-TNDs without US irradiation at the highest MI value of 1.50. As a control, naked DNA in the absence of nanodroplets was chosen to conduct the gene transfection experiment with the same US irradiation parameters. The results showed that naked DNA was difficult to transfect with or without US assistance, and the gene transfection efficiencies were 1.52×10^4 and 9.21×10^3 RLU/mg of protein, respectively. Therefore, we confirmed that the nanodroplets played an important role in enhancing gene transfection with US irradiation.

Conjoint analysis of the results of in vitro US imaging and gene transfection showed that US irradiation increased DNA transfection of nanodroplets, and this enhancement was related to the generation of microbubbles and their subsequent acoustic behaviors under various ultrasonic parameter settings. In Figure 6A,B, the better contrast effects could be noticed at 3.5 MHz compared with 2.5 MHz, revealing that more nanodroplets vaporized to microbubbles, resulting in improved cavitation. Additionally, when the MI value was gradually increased, the bubbles collapsed under US irradiation of higher MI to generate the stronger microjet for further improvement of cavitation and sonoporation, leading to significant enhancement of the gene transfection efficiency.

Note that, although the exposure time plays an important role for gene delivery according to some previous studies, the

DOI: 10.1021/acsami.5b02832
ACS Appl. Mater. Interfaces 2015, 7, 13524−13537

PFP-TNDs did not show the time-dependent transfection behaviors (Figure 7). For the samples at both 2.5 and 3.5 MHz, there was no significant difference among the different ultrasonic exposure times from 5 to 60 s. These results indicated that the process of ADV was instantaneous and the nanodroplets vaporized into microbubbles as much as possible within 5 s.

Finally, the multiway ANOVA was used to further evaluate the effect of the US frequency, MI, and exposure time on US-assisted gene transfection. Statistical analysis suggested that the factors of MI and frequency had a significant effect on the mean gene transfection efficiency ($p < 0.01$), while the factor of exposure time had no significant effect on the mean gene transfection efficiency ($p = 0.265$).

3.7. Cellular Uptake. Cellular uptake is a crucial step for gene carriers to realize gene delivery and transfection. First, it is essential to understand how the modifications by γ-PGA and PGA-*g*-mPEG influence the cellular uptake of the prepared nanodroplets, the PFP-BNDs and PFP-TNDs carrying fluorescence-labeling plamid interacted with HepG2 cells, and the intracellular fluorescence contents of the cells were detected by flow cytometry and CLSM. Figure 8 shows the results

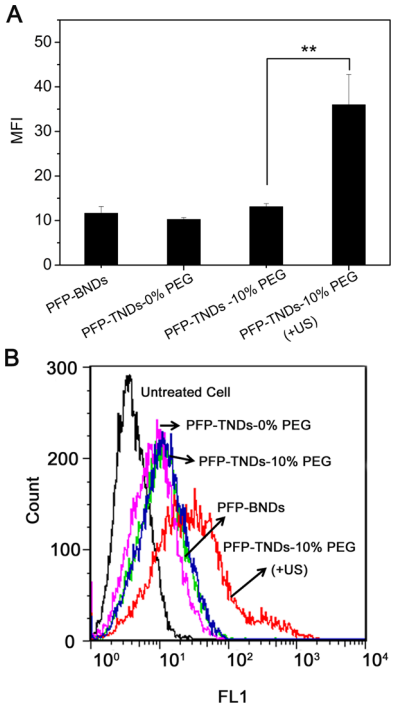

Figure 8. Quantitative analysis [MFIs (A) and fluorescence histograms (B)] of HepG2 cells by flow cytometry after cell incubation at various conditions: PFP-BNDs, PFP-TNDs−0% PEG, and PFP-TNDs−10% PEG (with or without US irradiation) bearing fluorescein-labeled LucDNA. Data are given as the mean ± standard deviation ($n = 3$). **: $p < 0.01$ (MI of 1.50, frequency of 3.5 MHz, and exposure time of 60 s).

obtained through flow cytometry, including the mean fluorescence intensity (MFI; Figure 8A) and fluorescence histogram (Figure 8B) after incubation for 4 h. Usually, nanoparticles with lower positive ζ potential are prone to having weaker electrostatic interactions with negative cell membranes, resulting in lower cellular uptake efficiency. However, despite its lower positive surface charge, the ternary nanodroplets PFP-TNDs modified by either γ-PGA or PGA-*g*-mPEG displayed the same level of MFI as the binary nanodroplets PFP-BNDs (Figure 8A). This similarity could also partially explain why PGA-*g*-mPEG modification did not decline the gene transfection efficiency (Figure 3B) because of the fact that the cellular uptake experienced a GGT receptor-mediated endocytosis process.[42,43] In addition, although excessive PEGylation has been thought to confine particles to interact with cells and reduce the cellular uptake rate,[35,41] the introduction of PEG to γ-PGA (10% PEG grafting) did not debase the cellular uptake efficiency of PFP-TNDs, revealing that the optimal content of PEG in PGA-*g*-mPEG was possibly not high enough to build a barrier for the interaction of nanodroplets and cell membranes.

Besides, the flow cytometry was also utilized to further investigate the effect of US on the promotion of cellular uptake. In Figure 8A, the cellular uptake of PFP-TNDs−10% PEG with labeled DNA was significantly increased approximately 3.5-fold by sonication than that of the same sample without US irradiation. On basis of analysis of previous studies, these results could be explained by the fact that US-assisted gene transfection enhancement is relevant to sonoporation of generating transient pores on the cell membrane.[54,55] It has also been reported that pores reseal in a few seconds following termination of US exposure.[56]

CLSM was selected to further study the cellular uptake process associated with PFP-loaded nanodroplets carrying fluorescein-labeled LucDNA (Figure 9). After 4 h of

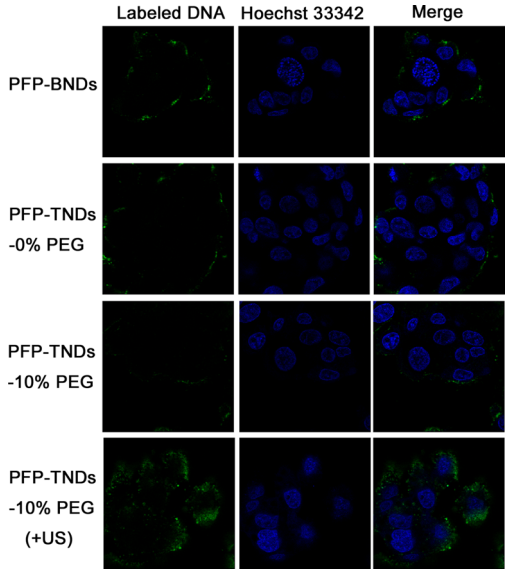

Figure 9. CLSM images of HepG2 cells incubated with the PFP-BNDs, PFP-TNDs−0% PEG, and PFP-TNDs−10% PEG (with or without US irradiation) carrying fluorescein-labeled LucDNA for 4 h (MI of 1.50, frequency of 3.5 MHz, and exposure time of 60 s).

incubation, the same level of low green fluorescence intensity was detected in the cells incubated with the PFP-BNDs and PFP-TNDs without US irradiation, which was consistent with the results of flow cytometry. As for the influence of US irradiation, the green fluorescence was much stronger for the groups treated with both PFP-TNDs and US. Thus, utilizing US is effective in promoting cellular uptake beneficial to the enhancement of gene transfection.

DOI: 10.1021/acsami.5b02832
ACS Appl. Mater. Interfaces 2015, 7, 13524−13537

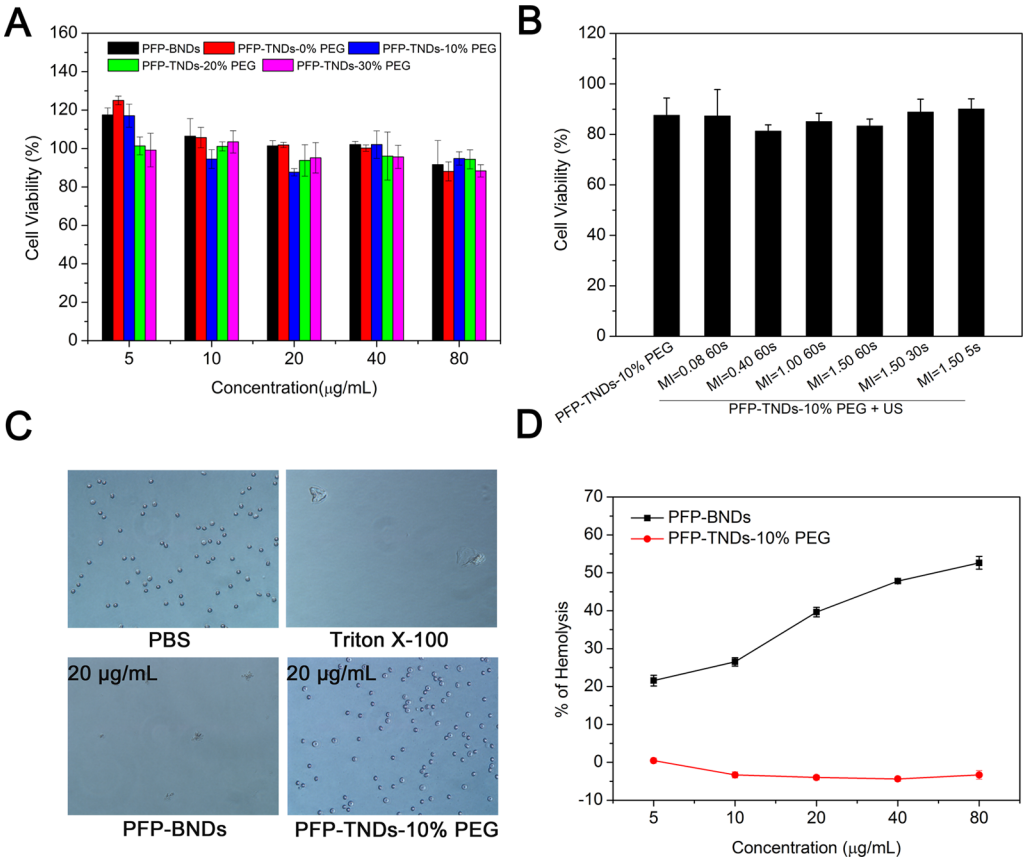

Figure 10. Cytotoxicity of the PFP-BNDs and PFP-TNDs modified with γ-PGA and PGA-*g*-mPEG carrying LucDNA: (A) cell viability of HepG2 cells 48 h after nanodroplet treatment at various concentrations, as detected by MTT assay; (B) cell viability of HepG2 cells after incubation with PFP-TNDs−10% PEG, followed by US irradiation under various ultrasonic conditions; (C) erythrocyte images after nanodroplet treatment at 20 μg/mL concentration using a microscope (400× magnification); (D) hemolytic activity of the nanodroplets at different polymer concentrations. Data are given as the mean ± standard deviation (n = 3).

3.8. In Vitro Cytotoxicity and Hemolysis Assay. The cytotoxicity of the PFP-BNDs and PFP-TNDs modified by γ-PGA and PGA-*g*-mPEG was assessed by MTT assay. As shown in Figure 10A, all of the samples showed no obvious cytotoxicity because of the fact that the cell viability of cells treated with each of these nanodroplets remained over 80% even at the highest nanodroplet concentration of 80 μg/mL. Moreover, the polymer concentration of 12.61 μg/mL was used in the gene transfection experiment, and the cell viability at this concentration was higher than 80%, confirming that the polymer for the gene transfection experiment had a negligible effect on the cytotoxicity. Besides, although the gene-delivery system PFP-TNDs−10% PEG built here showed better biocompatibility, during US irradiation, excessive sonoporation may cause a significant decrease of the cell viability. Therefore, the cytotoxicity of the PFP-TNDs−10% PEG with US irradiation was further detected on HepG2 cells by MTT assay. Considering the fact that a relatively higher MI value markedly influences the phase transition of nanodroplets, resulting in severe rupture of the microbubbles, and the high possibility of irreversible damage of the cell membrane, cytotoxicity was detected at various MI values ranging from 0.08 to 1.50. As shown in Figure 10B, there is no remarkable cytotoxicity for the PFP-TNDs−10% PEG, even at the highest MI value of 1.50. Additionally, the exposure time had also been taken into consideration, and the results proved no obvious decrease of the cell viability with exposure time within 60 s. Thus, the chosen US parameters and built experimental model in our study for the gene transfection experiment do not affect the cell proliferation, which is crucial for the gene-delivery system PFP-TNDs−10% PEG to be used for gene therapy with ultrasonic assistance.

Additionally, the PFP-BNDs and PFP-TNDs−10% PEG were incubated with erythrocytes to test the blood compatibility, and the morphology of the erythrocytes is displayed in Figure 10C, where Triton X-100 and PBS were selected as the positive and negative controls. Erythrocyte agglutination was visualized for the PFP-BNDs samples at a polymer concentration of 20 μg/mL but not observed for the ternary nanodroplets PFP-TNDs. The quantitative hemolysis analysis revealed that the ternary nanodroplets PFP-TNDs had negligible hemolytic activity even when the polymer concentration was increased to 80 μg/mL. In comparison, the hemolytic activity of PFP-BNDs was much higher than that of the ternary nanodroplets modified with PGA-*g*-mPEG even at lowest concentration (Figure 10D). Thus, the incorporation of PGA-*g*-mPEG effectively reduces the hemolytic activity of the cationic nanodroplets because of their decreased positive ζ potential after PGA-*g*-mPEG shielding.

4. CONCLUSIONS

We have developed a PFP-loaded US-triggered phase-transition cationic nanodroplet system for gene delivery consisting of the novel cationic polymer $C_{11}F_{17}$-PAsp(DET) as the core for

DOI: 10.1021/acsami.5b02832
ACS Appl. Mater. Interfaces 2015, 7, 13524−13537

loading PFP and DNA, a PGA-*g*-mPEG shell for nanoparticle stabilization, and enhancement of the biocompatibility and cellular uptake. In vitro studies demonstrated that the hydrophobic segment in $C_{11}F_{17}$-PAsp(DET) had high compatibility with PFP and the cationic hydrophilic segment successfully condensed DNA. The PGA-*g*-mPEG coating of the ternary nanodroplets PFP-TNDs decreased the positive surface charges, led to higher serum stability, and enhanced the cellular uptake efficiency through GGT receptor-mediated endocytosis. With US irradiation, microbubbles were generated, leading to a good US contrast effect. Besides, the gene transfection efficiency of PFP-TNDs−10% PEG was enhanced significantly against HepG2 cells mainly because of the better cellular uptake and US irradiation. These results demonstrate that the US-triggered phase-transition cationic nanodroplets can be utilized as efficient theranostic agents for targeting gene delivery.

■ ASSOCIATED CONTENT

Supporting Information

Optical images of PFP-TNDs−10% PEG samples at different temperatures, binding ability and acoustic stability of DNA for PFP-TNDs−10% PEG and PFP-BNDs, gene transfection efficiency of PFP-TNDs at different C/N ratios on LLC cells (GGT negative cell line), and the electrophoretic mobility of DNA in PFP-BNDs at different N/P ratios and PFP-TNDs−10% PEG at various C/N ratios. The Supporting Information is available free of charge on the ACS Publications website at DOI: 10.1021/acsami.5b02832.

■ AUTHOR INFORMATION

Corresponding Authors

*E-mail: wangw73@mail.sysu.edu.cn.

*E-mail: liujie56@mail.sysu.edu.cn.

Author Contributions

‡These authors contribute equally to this work.

Notes

The authors declare no competing financial interest.

■ ACKNOWLEDGMENTS

This work was supported by the Natural Science Foundation of Guangdong Province (Grant 2014A030312018), National Natural Science Foundation of China (Grants 51103183 and 81301238), the Project of Zhu Jiang Science & Technology New Star (Grant 2012J2200053), the Science and Technology Planning Project of Guangdong Province (Grants 2013B010404014 and 2012B091100452), and the Guangdong Innovative Research Team Program (Grant 2009010057).

■ REFERENCES

(1) Stone, D.; David, A.; Bolognani, F.; Lowenstein, P.; Castro, M. Viral Vectors for Gene Delivery and Gene Therapy within the Endocrine System. *J. Endocrinol.* **2000**, *164*, 103−118.

(2) Vasileva, A.; Jessberger, R. Precise Hit: Adeno-associated Virus in Gene Targeting. *Nat. Rev. Microbiol.* **2005**, *3*, 837−847.

(3) Check, E. Gene Therapy: A Tragic Setback. *Nature* **2002**, *420*, 116−118.

(4) Hacein-Bey-Abina, S.; Von Kalle, C.; Schmidt, M.; McCormack, M. P.; Wulffraat, N.; Leboulch, P.; Lim, A.; Osborne, C. S.; Pawliuk, R.; Morillon, E.; Sorensen, R.; Forster, A.; Fraser, P.; Cohen, J. I.; de Saint Basile, G.; Alexander, I.; Wintergerst, U.; Frebourg, T.; Aurias, A.; Stoppa-Lyonnet, D.; Romana, S.; Radford-Weiss, I.; Gross, F.; Valensi, F.; Delabesse, E.; Macintyre, E.; Sigaux, F.; Soulier, J.; Leiva, L. E.; Wissler, M.; Prinz, C.; Rabbitts, T. H.; Le Deist, F.; Fischer, A.; Cavazzana-Calvo, M. LMO_2-Associated Clonal T Cell Proliferation in Two Patients after Gene Therapy for SCID-X1. *Science* **2003**, *302*, 415−419.

(5) Raper, S. E.; Chirmule, N.; Lee, F. S.; Wivel, N. A.; Bagg, A.; Gao, G.-p.; Wilson, J. M.; Batshaw, M. L. Fatal Systemic Inflammatory Response Syndrome in a Ornithine Transcarbamylase Deficient Patient Following Adenoviral Gene Transfer. *Mol. Genet. Metab.* **2003**, *80*, 148−158.

(6) Ogris, M.; Brunner, S.; Schuller, S.; Kircheis, R.; Wagner, E. PEGylated DNA/transferrin−PEI Complexes: Reduced Interaction with Blood Components, Extended Circulation in Blood and Potential for Systemic Gene Delivery. *Gene Ther.* **1999**, *6*, 595−605.

(7) Zhou, J.; Liu, J.; Cheng, C. J.; Patel, T. R.; Weller, C. E.; Piepmeier, J. M.; Jiang, Z.; Saltzman, W. M. Biodegradable Poly(amine-*co*-ester) Terpolymers for Targeted Gene Delivery. *Nat. Mater.* **2012**, *11*, 82−90.

(8) Itaka, K.; Ishii, T.; Hasegawa, Y.; Kataoka, K. Biodegradable Polyamino Acid-based Polycations as Safe and Effective Gene Carrier Minimizing Cumulative Toxicity. *Biomaterials* **2010**, *31*, 3707−3714.

(9) Lin, S.; Du, F.; Wang, Y.; Ji, S.; Liang, D.; Yu, L.; Li, Z. An Acid-Labile Block Copolymer of PDMAEMA and PEG as Potential Carrier for Intelligent Gene Delivery Systems. *Biomacromolecules* **2007**, *9*, 109−115.

(10) Li, J.; Guo, Z.; Xin, J.; Zhao, G.; Xiao, H. 21-Arm Star Polymers with Different Cationic Groups Based on Cyclodextrin Core for DNA Delivery. *Carbohydr. Polym.* **2010**, *79*, 277−283.

(11) Xiu, K.; Yang, J.; Zhao, N.; Li, J.; Xu, F. Multiarm Cationic Star Polymers by Atom Transfer Radical Polymerization from Beta-cyclodextrin Cores: Influence of Arm Number and Length on Gene Delivery. *Acta Biomater.* **2013**, *9*, 4726−4733.

(12) Sato, T.; Ishii, T.; Okahata, Y. *In Vitro* Gene Delivery Mediated by Chitosan. Effect of pH, Serum, and Molecular Mass of Chitosan on the Transfection Efficiency. *Biomaterials* **2001**, *22*, 2075−2080.

(13) Yue, Y.; Wu, C. Progress and Perspectives in Developing Polymeric Vectors for *in Vitro* Gene Delivery. *Biomater. Sci.* **2013**, *1*, 152−170.

(14) Yang, Z.; Gao, D.; Cao, Z.; Zhang, C.; Cheng, D.; Liu, J.; Shuai, X. Drug and Gene Co-delivery Systems for Cancer Treatment. *Biomater. Sci.* **2015**, DOI: 10.1039/C4BM00369A.

(15) Ferrara, K.; Pollard, R.; Borden, M. Ultrasound Microbubble Contrast Agents: Fundamentals and Application to Gene and Drug Delivery. *Annu. Rev. Biomed. Eng.* **2007**, *9*, 415−447.

(16) Stratmeyer, M. E.; Greenleaf, J. F.; Dalecki, D.; Salvesen, K. A. Fetal Ultrasound: Mechanical Effects. *J. Ultrasound Med.* **2008**, *27*, 597−605.

(17) Suzuki, R.; Takizawa, T.; Negishi, Y.; Utoguchi, N.; Maruyama, K. Effective Gene Delivery with Novel Liposomal Bubbles and Ultrasonic Destruction Technology. *Int. J. Pharm.* **2008**, *354*, 49−55.

(18) Florinas, S.; Nam, H. Y.; Kim, S. W. Enhanced siRNA Delivery Using a Combination of an Arginine-grafted Bioreducible Polymer, Ultrasound, and Mmicrobubbles in Cancer Cells. *Mol. Pharmaceutics* **2013**, *10*, 2021−2030.

(19) Endo-Takahashi, Y.; Negishi, Y.; Nakamura, A.; Suzuki, D.; Ukai, S.; Sugimoto, K.; Moriyasu, F.; Takagi, N.; Suzuki, R.; Maruyama, K.; Aramaki, Y. pDNA-loaded Bubble Liposomes as Potential Ultrasound Imaging and Gene Delivery Agents. *Biomaterials* **2013**, *34*, 2807−2813.

(20) Yin, T.; Wang, P.; Li, J.; Zheng, R.; Zheng, B.; Cheng, D.; Li, R.; Lai, J.; Shuai, X. Ultrasound-sensitive siRNA-loaded Nanobubbles Formed by Hetero-assembly of Polymeric Micelles and Liposomes and Their Therapeutic Effect in Gliomas. *Biomaterials* **2013**, *34*, 4532−4543.

(21) Cavalli, R.; Bisazza, A.; Trotta, M.; Argenziano, M.; Civra, A.; Donalisio, M.; Lembo, D. New Chitosan Nanobubbles for Ultrasound-mediated Gene Delivery: Preparation and *in vitro* Characterization. *Int. J. Nanomed.* **2012**, *7*, 3309−3318.

DOI: 10.1021/acsami.5b02832
ACS Appl. Mater. Interfaces 2015, 7, 13524−13537

(22) Chin, L. S.; Lim, M.; Hung, T. T.; Marquis, C. P.; Amal, R. Perfluorodecalin Nanocapsule as an Oxygen Carrier and Contrast Agent for Ultrasound Imaging. *RSC Adv.* **2014**, *4*, 13052−13060.
(23) Rapoport, N. Y.; Kennedy, A. M.; Shea, J. E.; Scaife, C. L.; Nam, K. H. Controlled and Targeted Tumor Chemotherapy by Ultrasound-activated Nanoemulsions/microbubbles. *J. Controlled Release* **2009**, *138*, 268−276.
(24) Min, H. S.; Son, S.; Lee, T. W.; Koo, H.; Yoon, H. Y.; Na, J. H.; Choi, Y.; Park, J. H.; Lee, J.; Han, M. H.; Park, R.-W.; Kim, I.-S.; Jeong, S. Y.; Rhee, K.; Kim, S. H.; Kwon, I. C.; Kim, K. Liver-Specific and Echogenic Hyaluronic Acid Nanoparticles Facilitating Liver Cancer Discrimination. *Adv. Funct. Mater.* **2013**, *23*, 5518−5529.
(25) Yudina, A.; de Smet, M.; Lepetit-Coiffe, M.; Langereis, S.; Van Ruijssevelt, L.; Smirnov, P.; Bouchaud, V.; Voisin, P.; Grull, H.; Moonen, C. T. Ultrasound-mediated Intracellular Drug Delivery Using Microbubbles and Temperature-sensitive Liposomes. *J. Controlled Release* **2011**, *155*, 442−448.
(26) Diaz-Lopez, R.; Tsapis, N.; Libong, D.; Chaminade, P.; Connan, C.; Chehimi, M. M.; Berti, R.; Taulier, N.; Urbach, W.; Nicolas, V.; Fattal, E. Phospholipid Decoration of Microcapsules Containing Perfluorooctyl Bromide Used as Ultrasound Contrast Agents. *Biomaterials* **2009**, *30*, 1462−1472.
(27) Reznik, N.; Williams, R.; Burns, P. N. Investigation of Vaporized Submicron Perfluorocarbon Droplets as an Ultrasound Contrast Agent. *Ultrasound Med. Biol.* **2011**, *37*, 1271−1279.
(28) Sheeran, P. S.; Wong, V. P.; Luois, S.; McFarland, R. J.; Ross, W. D.; Feingold, S.; Matsunaga, T. O.; Dayton, P. A. Decafluorobutane as a Phase-Change Contrast Agent for Low-Energy Extravascular Ultrasonic Imaging. *Ultrasound Med. Biol.* **2011**, *37*, 1518−1530.
(29) Carneal, C. M.; Kripfgans, O. D.; Krücker, J.; Carson, P. L.; Fowlkes, J. B. A Tissue-Mimicking Ultrasound Test Object Using Droplet Vaporization to Create Point Targets. *IEEE Trans. Ultrason. Ferroelectr. Freq. Control* **2011**, *58*, 2013−2025.
(30) Zhang, M.; Fabiilli, M. L.; Haworth, K. J.; Padilla, F.; Swanson, S. D.; Kripfgans, O. D.; Carson, P. L.; Fowlkes, J. B. Acoustic Droplet Vaporization for Enhancement of Thermal Ablation by High Intensity Focused Ultrasound. *Acad. Radiol.* **2011**, *18*, 1123−1132.
(31) Schad, K. C.; Hynynen, K. *In Vitro* Characterization of Perfluorocarbon Droplets for Focused Ultrasound Therapy. *Phys. Med. Biol.* **2010**, *55*, 4933−4947.
(32) Wang, X.; Chen, H.; Zheng, Y.; Ma, M.; Chen, Y.; Zhang, K.; Zeng, D.; Shi, J. Au-nanoparticle Coated Mesoporous Silica Nanocapsule-based Multifunctional Platform for Ultrasound Mediated Imaging, Cytoclasis and Tumor Ablation. *Biomaterials* **2013**, *34*, 2057−2068.
(33) Daly, W. H.; Poché, D. The Preparation of *N*-carboxyanhydride of α-amino Acids Using Bis(trichloromethyl) Carbonate. *Tetrahedron Lett.* **1988**, *29*, 5859−5862.
(34) Poché, D. S.; Moore, M. J.; Bowles, J. L. An Unconventional Method for Purifying the *N*-carboxyanhydride Derivatives of γ-alkyl-L-glutamates. *Synth. Commun.* **1999**, *29*, 843−854.
(35) Zhang, X.; Tang, W.; Yang, Z.; Luo, X.; Luo, H.; Gao, D.; Chen, Y.; Jiang, Q.; Liu, J.; Jiang, Z. PEGylated Poly(amine-*co*-ester) Micelles as Biodegradable Non-viral Gene Vectors with Enhanced Stability, Reduced Toxicity and Higher *in vivo* Transfection Efficacy. *J. Mater. Chem. B* **2014**, *2*, 4034−4044.
(36) Nishihara, M.; Imai, K.; Yokoyama, M. Preparation of Perfluorocarbon/fluoroalkyl Polymer Nanodroplets for Cancer-targeted Ultrasound Contrast Agents. *Chem. Lett.* **2009**, *38*, 556−557.
(37) Shiraishi, K.; Endoh, R.; Furuhata, H.; Nishihara, M.; Suzuki, R.; Maruyama, K.; Oda, Y.; Jo, J.; Tabata, Y.; Yamamoto, J.; Yokoyama, M. A Facile Preparation Method of a PFC-containing Nano-sized Emulsion for Theranostics of Solid Tumors. *Int. J. .Pharm.* **2011**, *421*, 379−387.
(38) Liu, J.; Jiang, Z.; Zhou, J.; Zhang, S.; Saltzman, W. M. Enzyme-synthesized Poly(amine-*co*-esters) as Nonviral Vectors for Gene Delivery. *J. Biomed. Mater. Res., Part A* **2011**, *96*, 456−465.
(39) Gabizon, A. A.; Shmeeda, H.; Zalipsky, S. Pros and Cons of the Liposome Platform in Cancer Drug Targeting. *J. Liposome Res.* **2006**, *16*, 175−183.
(40) Gullotti, E.; Yeo, Y. Extracellularly activated nanocarriers: A New Paradigm of Tumor Targeted Drug Delivery. *Mol. Pharmaceutics* **2009**, *6*, 1041−1051.
(41) Yang, Z.; Jiang, Z.; Cao, Z.; Zhang, C.; Gao, D.; Luo, X.; Zhang, X.; Luo, H.; Jiang, Q.; Liu, J. Multifunctional Non-viral Gene Vectors with Enhanced Stability, Improved Cellular and Nuclear Uptake Capability, and Increased Transfection Efficiency. *Nanoscale* **2014**, *6*, 10193−10206.
(42) Liao, Z.-X.; Peng, S.-F.; Ho, Y.-C.; Mi, F.-L.; Maiti, B.; Sung, H.-W. Mechanistic Study of Transfection of Chitosan/DNA Complexes Coated by Anionic Poly(γ-glutamic acid). *Biomaterials* **2012**, *33*, 3306−3315.
(43) Lieberman, M. W.; Barrios, R.; Carter, B. Z.; Habib, G. M.; Lebovitz, R. M.; Rajagopalan, S.; Sepulveda, A. R.; Shi, Z. Z.; Wan, D. F. Gamma-Glutamyl transpeptidase. What Does the Organization and Expression of a Multipromoter Gene Tell Us about Its Functions? *Am. J. Pathol.* **1995**, *147*, 1175−1185.
(44) Zugates, G. T.; Anderson, D. G.; Little, S. R.; Lawhorn, I. E. B.; Langer, R. Synthesis of Poly(β-amino ester)s with Thiol-Reactive Side Chains for DNA Delivery. *J. Am. Chem. Soc.* **2006**, *128*, 12726−12734.
(45) Hannah, A.; Luke, G.; Wilson, K.; Homan, K.; Emelianov, S. Indocyanine Green-Loaded Photoacoustic Nanodroplets: Dual Contrast Nanoconstructs for Enhanced Photoacoustic and Ultrasound Imaging. *ACS Nano* **2014**, *8*, 250−259.
(46) Wilson, K.; Homan, K.; Emelianov, S. Biomedical Photoacoustics beyond Thermal Expansion Using Triggered Nanodroplet Vaporization for Contrast-enhanced Imaging. *Nat. Commun.* **2012**, *3*, 618.
(47) Rapoport, N.; Christensen, D. A.; Kennedy, A. M.; Nam, K. H. Cavitation Properties of Block Copolymer Stabilized Phase-shift Nanoemulsions Used as Drug Carriers. *Ultrasound Med. Biol.* **2010**, *36*, 419−429.
(48) Talu, E.; Hettiarachchi, K.; Zhao, S.; Powell, R. L.; Lee, A. P.; Longo, M. L.; Dayton, P. A. Tailoring the Size Distribution of Ultrasound Contrast Agents: Possible Method for Improving Sensitivity in Molecular Imaging. *Mol. Imaging* **2007**, *6*, 384−392.
(49) Hettiarachchi, K.; Talu, E.; Longo, M. L.; Dayton, P. A.; Lee, A. P. On-chip Generation of Microbubbles as a Practical Technology for Manufacturing Contrast Agents for Ultrasonic Imaging. *Lab Chip* **2007**, *7*, 463−468.
(50) Lin, P.-L.; Eckersley, R. J.; Hall, E. A. H. Ultrabubble: A Laminated Ultrasound Contrast Agent with Narrow Size Range. *Adv. Mater.* **2009**, *21*, 3949−3952.
(51) Deshpande, M. C.; Prausnitz, M. R. Synergistic Effect of Ultrasound and PEI on DNA Transfection *in vitro*. *J. Controlled Release* **2007**, *118*, 126−135.
(52) Elsner, H. I.; Lindblad, E. B. Ultrasonic Degradation of DNA. *DNA* **1989**, *8*, 697−701.
(53) Liu, C.; Chen, Z.; Yu, W.; Zhang, N. Novel Cationic 6-lauroxyhexyl Lysinate Modified Poly(lactic acid)−poly(ethylene glycol) Nanoparticles Enhance Gene Transfection. *J. Colloid Interface Sci.* **2011**, *354*, 528−535.
(54) Yang, F.; Gu, N.; Chen, D.; Xi, X.; Zhang, D.; Li, Y.; Wu, J. Experimental Study on Cell Self-sealing during Sonoporation. *J. Controlled Release* **2008**, *131*, 205−210.
(55) Qiu, Y.; Luo, Y.; Zhang, Y.; Cui, W.; Zhang, D.; Wu, J.; Zhang, J.; Tu, J. The Correlation between Acoustic Cavitation and Sonoporation Involved in Ultrasound-mediated DNA Transfection with Polyethylenimine (PEI) *in Vitro*. *J. Controlled Release* **2010**, *145*, 40−48.
(56) Zhou, Y.; Shi, J.; Cui, J.; Deng, C. X. Effects of Extracellular Calcium on Cell Membrane Resealing in Sonoporation. *J. Controlled Release* **2008**, *126*, 34−43.

DOI: 10.1021/acsami.5b02832
ACS Appl. Mater. Interfaces 2015, 7, 13524−13537